Fatigue Strength Upgrading of Cover Plate Ends by Welded Extensions in Existing Steel Bridge Girders

Vasileios Grigoriou
Scientist, School of Architecture, Civil and Environmental Engineering, Swiss Federal Institute of Technology in Lausanne, EPFL ENAC IIC RESSLAB, station 18, CH-1015 Lausanne. E-mail: vasileios.grigoriou@epfl.ch

Alain Nussbaumer
Adjunct Professor, School of Architecture, Civil and Environmental Engineering, Swiss Federal Institute of Technology in Lausanne, EPFL ENAC IIC RESSLAB, station 18, CH-1015 Lausanne. E-mail: alain.nussbaumer@epfl.ch

Dimitrios G. Lignos
Associate Professor, School of Architecture, Civil and Environmental Engineering, Swiss Federal Institute of Technology in Lausanne, EPFL ENAC IIC RESSLAB, station 18, CH-1015 Lausanne. E-mail: dimitrios.lignos@epfl.ch

Abstract: This paper investigates the fatigue upgrading of typical cover plate joint connections in existing steel bridge girders through cover plate extension. The upgraded detail is created by removing the existing transverse end weld, then welding the extension to the existing cover plate with the underlying plate acting as backing. The extended cover plate should end in a zone of low stress variation. The fatigue resistance of this detail is investigated by means of scaled specimen and beam testing as well as a corroborating detailed finite element parametric study. The different potential crack initiation sites as well as the three-dimensional effects due to the presence of longitudinal welds are considered. It is found that depending on the exact geometry of the joint, cracks may initiate either from the weld toe or the weld root. A classification of the joint in appropriate detail categories is proposed. It is shown that depending on the thicknesses of the cover plate extension, the existing cover plate and the underlying plate, the detail category may vary between FAT 50 and FAT 80 (E´ and D following AASHTO classification).

INTRODUCTION

Cover plates are occasionally fillet-welded on steel bridge girder flanges in order to increase their bending resistance. In most cases, these cover plates are discontinuous and located only in the regions of maximum/minimum moments, as shown schematically in **Fig. 1**. In these cases, the transverse welds at the cover plate ends introduce a particularly unfavorable stress concentration in the girder flanges. This joint type has a very low characteristic fatigue strength for nominal stress range, which, depending on the thicknesses of the underlying plate (flange) and the cover plate, ranges between 36 MPa and 56 MPa (AASHTO 2014; CEN 2005; Hobbacher 2016). Such a low fatigue strength may severely reduce the safe service life of a bridge. A possible intervention for upgrading the fatigue resistance of this joint type consists in extending the cover plate up to the next cover plate or up to a zone of low stress variation. This involves (i) the grinding of the transverse end welds and possibly a part of the existing cover plates, and (ii) fillet welding of the cover plate extensions to the underlying plate in the longitudinal direction and transverse butt welding of the connection with the existing cover plates and the girder flange in the transverse direction. The existing and upgraded joints are illustrated in **Fig. 2**.

Due to safety considerations, the traffic has to be interrupted during the intervention. The extension of the existing cover plate will not be stressed by the permanent loads and shall not be considered in the deflection computations at SLS; however, at ULS and fatigue limit state the entire cross-section including the extension should be considered. Regarding fatigue, the existing stress level will only marginally influence the upgraded connection performance because of grinding and re-welding; thus, one should conservatively assume high tensile residual stresses at the fatigue prone initiation points. The detail classification is solely done with the stress range that is typically used in most design standards. In the design of the upgraded joints, it might be desired to minimize the additional self-weight of the structure by using a cover plate extension thinner

than the existing cover plate. In that case, the difference in axial stiffness between the two plates results in that only a part of the axial force in the existing cover plate is transmitted to the extension, while the remaining part is deviated through the root of the transverse weld into the underlying plate. This flow of forces is schematically shown in **Fig. 2**. Because of the local force introduction, stress concentrations at the two boundaries of the weld root (i.e., R1 and R2 in **Fig. 2**) are not completely avoided in the upgraded joint. Their intensity depends on the magnitude of the deviated force and thus on the difference in thickness between the existing and the cover plate extension.

Thus, from a functional point of view, the proposed upgraded detail features characteristics of both a butt weld with backing and a transverse end weld. However, it differs from a butt weld with backing because the underlying plate, which plays the role of backing, directly attracts a significant portion of the applied load. It also differs from a transverse end weld because the region of stress concentration around root boundary R1 is delimited by the slit between the cover plate extension and the underlying plate and not by the obtuse notch of a weld toe. The influence of this geometry is examined in detail in this paper by means of detailed finite element simulation.

Kuhlmann and Kudla (2015) investigated a geometrically similar type of joint, the lamellae joint. They reviewed and analyzed a large set of experimental data and proposed the classification of this detail in category FAT 90 of EN-1993 (CEN 2005) (equivalent to category C in AASHTO LRFD Bridge design specifications (AASHTO 2014)), which is also the detail category for unground butt-welds with weld convexity height less than 10% of the weld width (CEN 2005). However, the aforementioned experiments were conducted on joints of packs of equal thickness or with a difference in thickness of less than 10%.

Other factors that may significantly affect the nominal fatigue strength of the upgraded joint include the longitudinal welds, which participate in the partial deviation of the axial force into the

underlying plate and restrict the extension plate from bending-away due to the weld root rotation (**Fig. 3**), and the grinding of the underlying plate (for the removal of the existing transverse end weld), which may introduce surface defects in the region of the new transverse weld root.

To the best of our knowledge, the nominal fatigue strength of the proposed detail is not covered by any of the details listed in the major fatigue design of welded structures standards including (AASHTO 2014; CEN 2005; Hobbacher 2016). The main objective of this paper is to suggest an appropriate classification of the proposed upgrading detail according to the size of its various components. This is achieved by taking into account all its above presented particular characteristics. This classification is accomplished by means of large-scale experiments complemented by detailed finite element parametric analysis.

EXPERIMENTAL INVESTIGATION

Specimens

The experimental program included the testing of 10 tensile specimens and 2 beam specimens. The specimens were fabricated from S355J2+N steel (nominal yield stress $f_y = 355$ MPa and minimum CVN value of 27 J at -20°C) according to an execution class EXC3 (CEN 2008). The specimens were fabricated in three stages in order to simulate the actual intervention in an existing steel bridge. After grinding to remove the existing welds and a small part of the existing cover plates, the longitudinal (non-fatigue critical) welds on both sides of the specimens were made in a second phase according to quality C requirements as per ISO 5817 (ISO 2014); the transverse butt welds were finally completed in a third phase according to quality class B requirements. A 25% portion of the class B welds was checked by Ultrasonic Testing. The transverse welds on the tensile specimens were executed in flat position, while the transverse welds on the beams (both flanges) were performed in overhead position in order to better simulate the welding conditions on site.

The specimens were inspected visually after the removal of the existing transverse end welds and of a small part of the cover plates, just before the welding of the additional cover plates. It was verified, by visual inspection, that the base plate surfaces (for the tensile specimens) or the flanges (for the beam specimens) close to the existing cover plates, where the transverse butt welds were about to be made, were smooth and free from visible grinding scratches. After the welding completion, there was no further treatment applied on the specimens except a very limited grinding of the plate edges as it can be seen in **Fig. 4**.

The geometry of the tensile specimens is shown in **Fig. 5(a)** and was adapted to the loading capacity and the dimensions of the testing machine and its hydraulic grips. Roughly speaking, the plate thicknesses used for the specimens are 2 to 3 times smaller than those usually encountered in real bridges. The dog-bone shape was necessary to ensure that the central part of the specimen had a sufficiently small sectional area such that the required stress levels could be applied without exceeding the load capacity of the testing machine. At the same time, the specimen extremities were sufficiently large such that the specimen could be properly clumped on the testing machine. The existing cover plate end was tapered with a slope of 1/4, which is the steepest slope generally allowed by most standards (AASHTO 2014; CEN 2005; Hobbacher 2016) in the similar fatigue detail descriptions. The specimens were instrumented with two strain gages (grid dimensions 5 mm × 10 mm), each one in a quarter bridge (3-wires) configuration. The strain gages were attached in the center of the cover plate extensions on each side of a specimen. The beam specimen geometry is shown in **Fig. 5(b)**. The beam specimens were designed for testing in four-point bending. Their dimensions were adapted to the capacity of the actuators and the dimensions of the available test setup. To this end, an IPE 270 profile was utilized (approximately equivalent to a W12×26), both flanges of which were reinforced using the above-described upgraded detail. It is

noted that due to the actuator capacity limitations the beam depth could not be scaled proportionally to the rest of the dimensions. Hence, the depth of the employed beams was 4 to 6 times smaller than what is usually encounter in real bridges, while the thicknesses and the flange width and cover plates are scaled down by a factor of approximately 1:2 to 1:3 as for the tensile specimens.

Testing parameters

Both tensile and beam specimens were tested under force-controlled constant amplitude cyclic loading with a loading ratio $R = 0.1$. The loading frequency f was different for each load amplitude and was chosen as the maximum frequency that could be sustained by the machine or the actuators in order to minimize the testing time (see **Tables 1 and 2**). Note that up to at least 50 Hz, the frequency has no effect on fatigue for steel at room temperature (e.g. Gurney 1979). The tensile specimens were tested at a universal testing machine, while the beam specimens were tested in a four-point bending set up whose geometry is shown in **Fig. 6**. Note that the two run-out specimens, T1 and T6, were retested at a higher load range. The results of these retests are identified under the names T1' and T6', respectively.

For the tensile specimens, the failure criterion was the fracture (complete separation) of the specimen, while for the beam specimens the failure criterion was the formation of a large crack affecting a large part of the bottom flange area; the two criteria are deemed equivalent.

The nominal stress range was calculated using the strain gage measurements installed in the center of the cover plate extensions on both the tensile and the beam specimens. For this purpose, a modulus of elasticity $E = 209$ GPa was deduced as the mean of $\Delta\sigma_1/[(\Delta\varepsilon_\mathrm{A} + \Delta\varepsilon_\mathrm{B})/2]$ for all the tensile specimens for which reliable strain measurements could be obtained; $\Delta\varepsilon_\mathrm{A}$ and $\Delta\varepsilon_\mathrm{B}$ are the strain ranges measured on the two sides, A and B respectively, of each specimen (see **Fig. 5(a)**).

By using direct strain measurements, the influence of the unintentional bending due to imperfections in the planarity of the specimens could be taken into account.

Depending on the observed failure mode, the nominal stress range was calculated either at the outer surface of the cover plate extension; or at the interface between base plate and cover plate; or at the surface of the weld between the two passes. It was assumed that a linear stress distribution in the cross-section is representative to determine nominal stress values for fatigue design (this applies to both the beam and the tensile specimens in which small bending moments develop during the test due to the inevitable non-planarity of the specimen). If strain gage measurements could not be obtained due to strain gage failures, the nominal stress range, for the tensile specimens, was calculated by simply dividing the applied force range ΔF by the initial nominal cross-sectional area A at the center of the tensile specimen. For the beam specimens, the same quantity was computed by dividing the moment range ΔM by the modulus of resistance $W_{\mathrm{y-y}}$ corresponding to the stress at the outer surface of the cover plate extension.

Observed failure modes

Three different failure modes were observed. Each one of them is characterized by a different location of the first crack initiation.

Most tensile specimens (T1', T2, T3, T5, T7 and T8) and the two beam specimens (B1 and B2) failed in a similar manner referred to as *Failure Mode I* and illustrated in **Figs. 7(a) and (b),** respectively. On one of the tensile specimen joints, multiple crack initiations at the toe (T) of the transverse weld coalesced and formed a large crack front, which propagated through the entire thickness of the extension cover plate. In parallel to the above crack propagation, cracks also initiated on the surface of the underlying plate at multiple locations along the root (R1) of the transverse weld. These cracks started to propagate rapidly once the cover plate fractured almost

through its entire thickness. Eventually, the final separation of the tensile specimen occurred with large plastification and necking of the opposite uncracked cover plate. In three of the above specimens (T3, T5, T8) crack initiations were also observed on the opposite surface of the underling plate along the weld root as well. Notably, these cracks had not propagated significantly at the time of the complete fracture of the base plate.

Specimens T4 and T6' failed in a different manner referred to as *Failure Mode II* and illustrated in **Fig. 7(c)**. In these specimens, a crack initiated between two passes on the surface of one of the transverse welds, and propagated through the weld itself and subsequently through almost the entire thickness of base plate forming a large flat crack propagation surface.

The failure mode of the remaining specimens T9 and T10 is referred to as *Failure Mode III* and is illustrated in **Fig. 7(d)**. In these cases, cracks initiated only at the root of the transverse weld and propagated simultaneously through the base plate and the weld. In specimen T9 some of the cracks initiated from air inclusions at the root of the weld. No damage nor crack initiation were detected in the longitudinal welds between the cover plate extension and main plate or flange of beam.

Results

The test data (summarized in **Table 3**) are fitted by linear regression to the logarithmic form of the classic $\Delta\sigma - N$ power relation $N = C(\Delta\sigma)^{-m}$. Where, N is the number of cycles to failure and m and C are the power law parameters. In accordance to the "Commentary to EC-3 – EN 1993 – Part 1-9 – Fatigue" (Sedlacek et al. 2014), the characteristic stress $\Delta\sigma_{C,0.05}$ is defined as the lower bound of the one-sided 5% prediction interval of $\Delta\sigma$ at 2.0E+06 cycles. The characteristic curve is defined as an offset of the regression line passing through point C (2.0E+06, $\Delta\sigma_{C,0.05}$). Only results with N<5E+06 are taken into account, i.e. only run-outs are excluded in this case (see Table 3). Calculations are performed for both a variable so-called "slope" and a fixed "slope" of $m = 3$.

Notably, in each specimen, there are more than one joints where fatigue failure can occur; four in the tensile specimens and two in the beams (considering the tension flange only). Thus, from a statistical point of view, a first-to-fail testing is used, the strength of the weaker location in the total length of the transverse weld beads being on average lower than in a single bead length. In order to be on the "safe" side this probabilistic "quantity-effect" (finite sample uncertainty) is not taken into account. In fact, this "quantity-effect" is rather welcomed in these tests since it makes the specimens more representative of the joints in real structures where the length of the beads is generally larger than the length of a single bead in the specimen and closer to the total length of the specimen beads.

The regression and statistical analysis is performed for five different data sets:

- *Subset 1* (T2, T3, T5, T7, T8) includes the data from the tensile specimens that failed in mode I, except T1′ that failed while retested at a higher load level after an initial run-out.
- *Subset 2* (T2, T3, T5, T7, T8, B1, B2) includes all the data of subset 1 plus the data from the two beam specimens.
- *Subset 3* (T2, T3, T5, T7, T8, T9, T10) includes the data from the tensile specimens that failed in modes I and III, i.e. the data of subset 1 plus the data from T9 and T10.
- *Subset 4* (T2, T3, T5, T7, T8, T9, T10, B1, B2) includes all the data of subset 3 plus the data from the two beam specimens.
- *Full set 5* (T1', T2, T3, T4', T5, T6, T7, T8, T9, T10, B1, B2) comprises all the available data including those from specimens retested at higher load after a run-out.

The calculated $\Delta\sigma - N$ curve parameters and characteristic strengths are summarized in **Table 4** for all the five subsets and plotted in **Fig. 8** for the *Full set*.

Discussion

When only the results from tests in which the first crack initiation occurred at the weld toe are taken into account (Subsets 1 and 2), the resulting characteristic stress $\Delta\sigma_{C,0.05}$ is approximately equal to 100 MPa. To some extent, this relatively high strength is due to the small thickness of the specimens, which is much less than the reference thickness of 25 mm for which detail categories are generally determined.

It can also be noted that when only data from the tensile specimens are considered (i.e. Subset 1), the determined slope m of the $\Delta\sigma - N$ curve is substantially greater than the standard slope $m = 3$; however, when the data from beam specimens are also included, a slope closer to $m = 3$ is obtained. It is not clear whether this difference suggests a longer crack initiation period in the tensile specimens or is due to the small number of data in Subset 1.

The fact that in most specimens cracks initiated first from the transverse weld toe, suggest that for the particular specimen geometry the nominal fatigue strength of the weld toe (estimated above as $\Delta\sigma_{C,0.05} = 100$ MPa) is lower than that of the weld root. At the same time, the fact that, in all the specimens, cracks initiated also from the weld root – more often as secondary cracks but in some cases also as primary cracks – indicates qualitatively that the observed strength of the weld root is not much higher than that of the weld toe. Unfortunately, the two specimens (T9 and T10) in which cracks first initiated at the weld root are too few to allow for a rigorous quantification of the weld root resistance. When the results from these two tests are included in the statistical analysis, the characteristic stress $\Delta\sigma_{C,0.05}$ becomes less than 90 MPa. This decrease is mainly due to the increased standard error s of the regression, while, a median stress $\Delta\sigma_C$ is not significantly different and has, in fact, a slightly higher value (compare for instance Subset 1 to Subset 3 and Subset 2 to Subset 4).

The above observations suggest that for different thickness combinations and larger specimens the fatigue strength of the weld root may become critical. This issue is treated in the following section by means of numerical analyses through detailed finite element modeling.

NUMERICAL INVESTIGATION

By means of the following numerical investigation (conducted using ANSYS 16.2), the findings of the experimental investigation are extended to cases that involve thicker plates and different thickness ratios by explicitly taking into account the geometric size effect. The type of size effect investigated by means of FE analyses originates from the fact that the microstructural geometry of the material remains unscaled while the macroscopic geometry of the detail is scaled. Additionally, the three-dimensional effect introduced by the longitudinal welds is quantified by comparing results from 3-Dimensional (3D) and 2-Dimensional (2D) Finite Element (FE) models.

FE modeling

The developed FE models correspond to the general geometric configuration of the central part of the tensile specimens (i.e. the constant width part). This is, in fact, the geometry of a doubly symmetric joint with cover plates welded on both sides of a single middle (underlying) plate and the two cover plate "extensions" placed centrally on the underlying plate. This geometric configuration is characterized by two symmetry planes: the middle plane of the underling plate and cross section plane passing from the middle of the cover plate extension. As a consequence, only 1/4 or 1/8 of the joint needs to be modeled in 2D and/or in 3D, respectively, with appropriate boundary conditions applied on the nodes on the symmetry planes. The general geometry, boundary conditions and loading of the FE models are illustrated in **Fig. 9**. The nominal stress is defined as the mean stress over the X-X symmetry cross-section (i.e. in the thinner part of the joint). However, the loading is applied on the free end of the model. The value of the applied stress

p is calculated as shown in **Fig. 9** so that the nominal stress as defined above has a value of 100 Pa. In **Fig. 10**, the simplified model geometry is superimposed to the cross section of one representative specimen. A number of simplifications are made in the model geometry in comparison to the actual geometry of the specimens.

First, the actual shape of the weld reinforcement is not included in the model. Instead, a constant slope of ¼ (166°) is used in all the analyzed cases regardless of the plate thicknesses. Measurements of the actual angle of the weld toe in five out of ten fractured joints in the tensile specimens show a range of 158°-164°, with a mean of 161.7° and a standard deviation of 2.5°. The angle was also measured in one of the two fractured joints in the beam specimens and found equal to 150°−the lower value may be related to the overhead welding position. The measured local angles are similar to the angle of the overall slope used in the model, so that the above simplification is deemed representative of both the overall and the local geometry of the weld toe. Additionally, it is assumed that the weld toe is located (T) just above the weld root (R1).

The width of the weld root has a significant impact on the calculated results. For its realistic specification, five of the specimens were cut in order to measure the actual width of the weld root. The measured root widths show a relatively large scatter ranging from 8 to 14 mm with a mean value of approximately 11 mm. Using the minimum observed root width of 8 mm and given that the prescribed gap between the plates was 3 mm, a fusion width of (8-3)/2 = 2.5 mm on each side of the root is assumed. This suggests that the actual gap applied during the fabrication of the specimens had a mean value of 11-5 = 6 mm, approximately equal to the thickness of the extension cover plate. In the FE model of the specimen the observed mean value of the root width is employed. For the parametric analysis, it is additionally specified that the gap between the plates

increase proportionally to the thickness of the extension cover plate, while the fusion depth remains constant. Hence, the width of the root e is determined as $t_{c2} + 5$ mm.

In order to achieve the mesh refinement required for the application of the local stress method described below, the sub modeling technique is utilized. The sub-modeled regions around the weld toe and the weld root boundaries are shown in **Fig. 9**. Typical meshes for both the global and the sub-models are shown in **Fig. 11**. In general, mapped meshing with quadrilateral or hexahedral elements is applied except for the modeling of the longitudinal welds and the tapered part of the cover plate in the 3D models. The angle of the longitudinal welds with the base plate is taken equal to 45° and the fillet contact dimension is taken equal to the thickness of the cover plate extension minus 1 mm (in order to facilitate the parametric definition of the geometry); no fusion has been assumed. Linear elements with full integration are used in the global models and quadratic elements with reduced integration in the sub-models. Each sub-model contains an inner region meshed with elements of size equal to 0.05 mm and an outer region in which the size of the elements increases progressively.

In the FE model, the cover and underlying plates are allowed to separate. It is therefore necessary to model the contact behavior. This is achieved using contact and target elements (CONTA 172 & TARGE 169 for 2D analysis and CONTA 173 & TARGE 170 for 3D analysis). Asymmetric contact is applied with the contact elements overlaying the internal cover-plate surfaces and target elements overlying the underlying plate surfaces. Contact is assumed frictionless and cohesionless. A penalty based augmented Lagrange formulation is employed. This formulation allows for a small controlled penetration, but eliminates the phenomenon of chattering (contact points oscillating between close and open position), which often occurs in the alternative normal Lagrange formulation, which does not allow penetration. The normal contact stiffness

value is set to 1 (a value that is suitable for bulk deformation), while the penetration tolerance is set to 0.1 of the underling element thickness. It has been verified that the calculated values of the Stress Concentration Factor (SCF) (see below) are not sensitive to the value of the penetration tolerance factor (for example, when this factor is reduced to 0.05, the change in the SCF is less than 1%). In general, contact is a non-linear phenomenon. However, in this case, once a low load level is exceeded and the contact areas are numerically established, the FE model response becomes essentially linear with the contact area remaining practically unchanged and the load increase leading only to a proportional increase in the contact pressure. The applied pressure of 100 Pa is sufficient for the establishment of the contact areas. It has been verified that the contact response of the models is not affected when smaller elements are employed. Contact elements are not used in the sub-models, because the part of the plate interface included in the sub-models is either completely separated (R1), in which case no boundary conditions are imposed on the two surfaces of the interface, or completely in contact, in which the nodes on the two surfaces of the interface are coupled in the Y direction so that contact pressure can be transmitted while relative sliding remains unrestricted.

In all the above models a linear material model is assumed. Second order effects are neglected.

Calculation of fatigue strength by local stress methods

The geometric size effect, for crack initiation and early crack propagation, can only be fully considered through a local Stress Concertation Factor (SCF), which relates the fatigue strength of the joint for a nominal stress range to the steel material's fatigue strength for local stress range. The material fatigue strength for local stress range is independent, of course, of the joint geometry but dependent on the exact definition of the local stress and the geometry involved in this definition.

In this paper, the local stress is defined, following the Point Method of the Critical Distance approach (CD-PM) (Taylor et al. 2002), as the first principal stress at distance r_c from the weld toe or the weld root, in the direction in which this principal stress is maximum. The length r_c is a material property equal to 1/2 of the El-Haddad material characteristic length (El Haddad et al. 1979) a_0:

$$r_c = \frac{a_0}{2} = \frac{1}{2\pi}\left(\frac{\Delta K_{th}}{\Delta \sigma_0}\right)^2 \quad (1)$$

In which, $\Delta\sigma_0$ is the fatigue limit (in terms of stress range); and ΔK_{th} is the threshold value of the Stress Intensity Factor (SIF) range. Because the possibility of defining the above properties in an absolute way is questionable, the values of $\Delta\sigma_0$ and ΔK_{th} for use in the above expression are defined as the fatigue strength at 5.0E+06 cycles of plane and sharply notched specimens of ground-flush butt-welds in terms of stress range and SIF range respectively. Using data from the literature (Taylor et al. 2002; Livieri and Lazzarin 2005) a value of $r_c = 0.21$ mm is established. In the parametric analyses that follow, square elements of size 0.05 mm are used for the modeling of the region around the toe and the root boundaries. Given this fixed discretization pattern the exact nodal locations at which the principal stress is evaluated are shown in **Fig. 12**. The nodal location distance from the notch tip is slightly different than the above calculated distance r_c. Also, the directions along which the distance is measured do not perfectly coincide with the directions of maximum principal stress but are fixed as shown in **Fig. 12**. The error introduced by these approximations is negligible considering the uncertainty related to the value of r_c.

In the 3D models the least favorable stress field around the weld root occurs on the Z-Z plane of symmetry (i.e. on the longitudinal section at Z=0), while the least favorable stress field in the weld toe occurs near the longitudinal weld at a distance of approximately 1/10 of the plate width from it. Hence, the sub-models around the root boundaries are always adjacent to the symmetry

plane, while the exact position of the weld toe sub-model is determined after the analysis of the corresponding global model as the distance at which the maximum surface stress along the weld toe occurs.

After the calculation of the local stress according to the CD-PM, σ_{CD-PM}, the local SCF is calculated by dividing the local stress by the nominal stress σ_{nom}. The fatigue strength of the joint for the nominal stress range is then calculated by dividing the fatigue strength of the material for local stress range by the SCF. According to Taylor et al. (2002), the material fatigue strength for application with the CD-PM in the case of welded joints can be considered equal to the fatigue strength of ground-flush transverse butt welds of the same materials. According to EN 1993-1-9 (CEN 2005) and the IIW Recommendations (Hobbacher 2016), ground-flush transverse butt welds are classified in detail category FAT 112. A misalignment factor of 1.15 is already included in this category (Hobbacher 2016). In the case of the investigated joint, misalignment can be excluded because both cover plates lie on the same underlying plate. Hence, the value $1.15 * 112 = 128.8$ MPa can be considered as a lower bound for the 5% characteristic fatigue strength of the material for local stress range at 2.0E+06 cycles (corresponding to $\Delta\sigma_{\mathrm{C},0.05}$). An upper bound of 143.7 MPa, corresponding to the next higher detail category FAT 125, could also be considered. Taylor et al. (2002) determined experimentally the mean fatigue strength at 2.0E+06 cycles of ground-flush butt welds on low carbon steel approximately equal to 182 MPa. Kuhlmann and Kudla (2015) determined the $\Delta\sigma_{\mathrm{C},0.50}/\Delta\sigma_{\mathrm{C},0.05}$ ratio from tests on lamellae joints approximately equal to 1.35. Therefore, a value 183/1.35=**135 MPa** can be calculated for the 5% characteristic fatigue strength of the material for local stress range at 2.0E+06 cycles; this value falls within the above bounds and is employed from this point on.

The fact that the local stress has to be evaluated at such a small distance from a point of theoretical singularity implies that a very fine discretization of the stress concentration region is required in order to obtain accurate results from a finite element simulation. This is the main drawback of the above method. For this reason, the authors tried also to utilize an alternative approach developed by Meneghetti & Lazzarin (2007). This approach allows for the calculation of a representative local stress from that obtained at the theoretical singularity point, by mean of a rather coarse discretization. The method is based on the hypothesis that the fatigue resistance can be expressed in terms of the average Elastic Strain Energy Density (ESED) in a representative cylindrical volume surrounding the notch tip; the representative stress is defined as the uniaxial stress, in plane strain conditions that corresponds to the same ESED. Additionally, it is assumed that the stress field around the notch tip can be expressed as the result of the superposition of a symmetric opening loading (mode I) and an antisymmetric shearing loading (mode II) and that the elastic strain energy in the cylindrical volume can be expressed analytically in terms of the Notch Stress Intensity Factors (N-SIF) K_{I} and K_{II}, for mode I and II, respectively. This assumption is shown to be valid in large but limited range of cases in which the contribution of higher order non-singular terms (e.g. T-stress) in the stress field near the notch tip can be neglected. Furthermore, it is shown that under certain limitations the N-SIFs can be calculated from the peak stress resulting from a rather coarse mesh by taking into account this element size and using an empirical factor K_{FE}^{*}, which depends on the element type but has very little variation for a large range of notch opening angles (0° to 135°).

Because of the practical advantages of the above method, the validity of the above hypotheses in the case of the proposed joint is examined. It is found that at the weld root the energy calculated analytically from the N-SIFs is significantly lower than the energy calculated numerically from a

finite element model with adequate mesh refinement around the notch tip (R1). This is attributed to the presence of a significant nonsingular stress field parallel to the notch (i.e. the plate length). The influence of this field can be illustrated by considering the limiting case in which a crack lies parallel to a uniaxial uniform stress σ_x in 2D plane strain conditions. In this case, $K_I = K_{II} = 0$ and the analytical expression would predict zero ESED. However, the ESDE in this case has in fact, a uniform value of $(1-\nu^2)\sigma_x^2/2$. Another problem related to the application of the peak stress method in the present joint is that the notch opening angle at the weld toe (162° in average) lies outside the range in which the empirical factor K_{FE}^* remains nearly constant. Consequently, it was found that the peak stress method, in its above mentioned formulation, cannot be employed in the context of this work.

Validation of the assumptions of the numerical fatigue strength calculation

By applying the aforementioned procedure for a joint with the geometry of the tested tensile specimens, the following fatigue strengths for nominal stress range are obtained for the three locations of possible crack initiation: weld toe (T) $\Delta\sigma_{C,0.05} = 96$ MPa, weld root (R1) $\Delta\sigma_{C,0.05} = 103$ MPa, weld root (R2) $\Delta\sigma_{C,0.05} = 111$ MPa. These results suggest, in qualitative and quantitative accordance with the experimental findings, that the most probable crack initiation location is the weld toe followed, but only with a small difference, by the weld root at R1. Moreover, the fatigue strength obtained for the weld toe is only 4% lower than the characteristic strength obtained experimentally considering only the specimens in which cracks initiated from the weld toe (100 MPa for subsets 1 and 2 above).

PARAMETRIC ANALYSIS

Investigated cases

Taking into account the geometric simplifications presented in Section 3, eighteen different geometries are considered. These cases include two ratios of existing cover plate thickness to base plate thickness t_{c1}/t_b (1.2 and 0.75), three ratios of extension cover plate thickness over existing cover plate thickness t_{c2}/t_{c1} (0.5, 0.67 and 0.75) and three existing cover plate thicknesses t_{c1} (12 mm, 30 mm and 50 mm). For each case, the plate thicknesses t_b, t_{c1}, t_{c2}, the width of the root e, the element size D of the global FE model, the size L of the sub model are listed in **Table 5**. Case 1 corresponds to the geometry of the tested tensile specimens. For all sub-models the element size d is taken equal to 0.05 mm.

All the cases are analyzed using 3D FE models with which the restraint imposed on the cover plates by the longitudinal welds is naturally taken into account both near the middle of the plate, where the SCF is maximum for the weld root, and near the longitudinal welds, where the SCF is maximum for the weld toe.

In order to investigate the relative importance of the 3D effects, six of the above cases are also analyzed by means of 2D FE models (**Table 6**). For the 2D analyses, three different hypotheses for the interaction of the plates at their interface are considered. According to the first hypothesis, which in **Table 6** is named "2D merged", the underlying plate and the cover plates are merged together and there is no interface; it is representative of the conditions along the longitudinal welded sides of the cover plates and can be used in order to calculate the local stress at the transverse weld toe near the longitudinal welds. However, under the above hypothesis, it is not possible to define a weld root and for that reason, the corresponding models cannot be employed for fatigue strength evaluation of the weld root. According to the second hypothesis ("2D contact"), the plates are allowed to separate and to slide one relatively to the other without any external retain (e.g. from virtual springs). This condition is modeled by means of contact elements

and can be considered as a lower bound (conservative) approximation for the fatigue strength evaluation at the weld root away from the longitudinal welds; on the other hand, it should not be used for the evaluation of the fatigue strength of the weld toe, since the stress concentration at the toe is much higher near the longitudinal weld and decreases towards the middle of the cover plate. The third hypothesis, which is named "2D bonded", is that the plates are allowed to slide one relatively to the other but are not allowed to separate. This hypothesis does not correspond to the actual conditions at any longitudinal section of the joint; however, it allows the definition of the weld root and for this reason it is examined here as a potentially useful approximation, which could make possible the fatigue strength calculation at both the weld toe and the weld root using a single 2D-model.

Results and discussion

The results of the parametric analysis are presented in **Tables 5 and 6** for the 3D and 2D models, respectively. The results are presented in terms of the SCF and the 5% characteristic nominal fatigue strength for the weld toe and the two borders of the weld root, calculated according to Section 3.2.

Notably, the nominal fatigue strength of the weld toe depends mainly on the sum of the thicknesses of the underlying plate and the extension cover plate, as it can be seen in **Fig. 13(a)**, while it has very little dependence on the cover plate thickness ratio. On the other hand, the fatigue strength of the weld root increases with t_{c2}/t_{c1} and decreases with t_b, as it can be seen in **Fig. 13(b)**. In general, the root strength becomes critical for smaller t_{c2}/t_{c1} and larger t_b. The site R1 is always more critical than R2.

The comparison with the 2D results shows that the 2D merged models provide rational results for the weld toe, while the 2D contact models provide consistent but conservative results (as

expected). Furthermore, it is noted that the SCFs for the weld toe calculated according to the 2D contact method are severely underestimated (and generally below unit). For this reason, they are not reported in **Table 6**. As for the 2D coupled models, they: a) severely underestimate the toe strength, b) overestimate the root strength, and, contrary to the experimental findings, c) predict first crack initiation from R2. Hence, when applying 2D analysis, two different models, "2D-merged" and "2D-contact", have to be utilized for the calculation of the fatigue strength of the weld toe and weld root, respectively. Contrary to what was originally speculated, the "2D-coupled" model does not provide realistic results.

RECOMMENDATIONS FOR PRACTICAL APPLICATIONS

For design purposes, the fatigue strength of the upgraded joint for nominal stress range is classified in detail categories according to **Table 7**. The nominal stress range is defined at the outer face of the additional (thinner) cover plate. This definition takes into account the global bending of the beam whose flanges are reinforced using the proposed detail (i.e. the nominal stress being slightly lower at the weld root). The recommended classes are defined by ranges of the underlying plate thickness and of the ratio of the extension cover plate thickness over the existing cover plate thickness. The classification is based on the categories defined by EN 1993-1-9 (CEN 2005), while the corresponding categories according to AASHTO LRFD Bridge Design Specifications (AASHTO 2004) are given in parenthesis (the following correspondence applies in general: 160 (A); 140, 125 (B); 112, 100 (B′); 90 (C); 80, 71 (D); 63, 56 (E); 50, 45, 40 (E′)). This classification takes into account the lowest strength between the weld root and the weld toes strength. The classes in which the weld root strength is critical are denoted with an asterisk. Note that some of the above-calculated cases that fall within a class with asterisk may have almost the same strength for both the toe and root (in fact, the toe strength may even be slightly lower than that of the root). This is

due to the higher sensitivity of the root strength to the geometric parameters and to the fact that the overall strength of each class corresponds to the most unfavorable geometry within the class.

The above recommendations are valid within the range of geometries covered by the 3D parametric analysis discussed in the previous section. For geometries outside this range only provisory recommendations can be provided. In particular, when the sum of the underlying plate thickness and the extension cover plate thickness exceeds 70 mm, the fatigue strength of the classes without an asterisk in **Table 7** should be downgraded by one FAT category. Additionally, given the 2D analyses results, it is recommended that when the cover plate extension width exceeds 15 times the thickness of the extension cover plate, then the fatigue strength of the classes with an asterisk in **Table 7** should be downgraded by one FAT category. There is no additional size effect factor to be taken into account.

The above classification requires that the following recommendations related to the execution of the joint be observed. Quality class B (ISO 2014) should be ensured for the transverse butt welds between existing and additional cover plate. In addition, any interpass undercut should be eliminated by grinding. In order to ensure that a crack that might have already initiated from the eliminated welds of the existing cover plate will not be permanently covered by the extension cover plate, dye Penetrant Testing (PT) should be performed at the location of these welds after grinding. It should also be ensured that the ground surface of the underlying plate or flange is smooth, free from scratches and remains shallow (< 1 mm undercut). Additional geometric constraints are given in **Fig. 14**. Note that a sufficiently large gap for the weld root is required mainly in order to reduce the stress concentration but also to facilitate the execution of the weld root and to improve its quality.

CONCLUSIONS

In this paper the main findings of a study on the fatigue resistance of a joint detail that can be used for the fatigue strength upgrading of cover plate ends in existing steel bridge girders are presented. Because of their low fatigue strength, cover plate ends may adversely affect the durability of a bridge and may have to be retrofitted. The upgrading involves the elimination of the existing transverse end weld by grinding and the welding of a cover plate extension with the underlying plate acting as backing. Based on the findings from the coordinated experimental and analytical research work, recommendations for the classification in detail categories of the fatigue strength of the upgraded joint for nominal stress range were proposed for practical applications. The determined fatigue categories account for the size effect and cover a large range of plate thicknesses encountered in practice.

The main findings of this paper are summarized as follows:

- In most of the specimens, cracks initiated first from the weld toe, but indications of cracks initiating and propagating from the weld root were also observed on the fracture surfaces (Mode I failure). In two specimens cracks also initiated from the surface between two passes (Mode II failure); however, for the determination of the fatigue category it is assumed that appropriate measures are taken into consideration in order to eliminate the probability of crack initiation between passes (grinding).
- The fatigue resistance of the examined joint can be considered as the minimum fatigue resistance of the weld toe and that of the weld root. For the relatively small joint thicknesses that were tested, the weld toe resistance was critical. However, complementary numerical analyses indicate that for larger joints the resistance of the root may become critical if the existing and the additional cover plate have different thicknesses. When the root becomes critical, a severe reduction in the fatigue strength of the detail may occur.

- The presence of the longitudinal welds introduces a significant 3-dimentional (3D) effect in the joint. However, 2-dimensional (2D) FE models can also be employed in order to obtain lower bounds of the fatigue resistance. In this case, two models with different interface conditions, "merged nodes" and "contact elements", should be utilized for the fatigue strength calculation of the weld toe and weld root, respectively.
- Depending on the thicknesses of the cover plate extension, the existing cover plate and the underlying plate, the detail category may vary between FAT 50 and FAT 80. (E′ and D following AASHTO classification).
- In order to minimize the possibility of crack initiation from the weld root it is recommended to consider a joint with equal thickness for the existing and the additional cover plate.

ACKNOWLEDGEMENTS

This research project was financed by the Swiss Federal Railways (CFF SA). The authors wish to thank CFF SA engineers Alexandre Michon and Jean-Jacques Reber for the fruitful discussions and practical propositions made during the course of this research project as well as the experimental report drafting. They also wish to thank Martina Paronesso for her help in the final preparation of the paper. Financial support was also provided by Ecole Polytechnique Fédérale de Lausanne (EPFL) for the completion of the finite element studies discussed in the paper. Any opinions, findings, and conclusions or recommendations expressed in this paper are those of the authors and do not necessarily reflect the views of sponsors.

REFERENCES

AASHTO (American Association of State Highway and Transportation Officials). (2014). *LRFD Bridge Design Specifications - 7th ed.*

CEN (European Committee for Standardization). (2005). “Eurocode 3: Design of steel structures – Part 1-9: Fatigue.” *EN1993-1-9*, Brussels.

CEN (European Committee for Standardization). (2008). “Execution of steel structures and aluminium structures – Part2: Technical requirements for steel structures.” *EN 1090-2:2008*, Brussels.

El Haddad, M. H., Topper, T. H., and Smith, K. N. (1979). “Prediction of non propagating cracks.” *Engineering Fracture Mechanics*, 11(3), 573-584.

Gurney, T. R. (1979). "Fatigue of Welded Structures," 2nd Edition, Cambridge University Press, Cambridge.

Hobbacher, A. (2016). “Recommendations for Fatigue Design of Welded Joints and Components – Second Edition.” *IIW (International Institute for Welding)-2259-15*, Springer.

ISO (International Organization for Standardization). (2014). “Welding - Fusion-welded joints in steel, nickel, titanium and their alloys (beam welding excluded) - Quality levels for imperfections.” *ISO 5817*.

Kuhlmann, U., and Kudla, K. (2015). “Ermüdungsfestigkeit von Lamellenstößen bei Vollwandträgern mit dicken Gurten - Experimentelle und numerische Untersuchungen [Fatigue resistance of lamella joints of plated steel girders with thick flanges – experimental and numerical investigations].” *Stahlbau*, 84(3), 203-212 (in German).

Livieri, P., and Lazzarin, P. (2005). “Fatigue strength of steel and aluminium welded joints based on generalised stress intensity factors and local strain energy values.” *Int. J. Fracture*, 133(3), 247-276.

Meneghetti, G., and Lazzarin, P. (2007). “Significance of the elastic peak stress evaluated by FE analyses at the point of singularity of sharp V-notched components.” *Fatigue & Fracture of Engineering Materials & Structures*, 30(2), 95-106.

Sedlacek, G., Hobbacher, A., Nussbaumer, A., Stötzel, J., and Schäfer, D. (2014). "Commentary to EC-3 – EN 1993 – Part 1-9 – Fatigue." Citarelli, S., Eichler, B., Feldmann, M., eds., RWTH AACHEN Stahlbau University, Aachen.

Taylor, D., Barrett, N., and Lucano, G. (2002). "Some new methods for predicting fatigue in welded joints." *Int. J. Fatigue*, 24(5), 509-518.

Figure Captions

Fig. 1. A steel girder locally reinforced at the regions of maximum/minimum moment by cover plates welded on the flanges.

Fig. 2. Existing transverse end weld and upgraded joint with illustration of the flow of forces

Fig. 3. Deformed shape of the detail under tensile load showing the cover plate bending away the underlying plate due to the indicated rotation of the root.

Fig. 4. Transverse weld between existing and extension cover plates in specimen T3. Typical of all transverse welds on all specimens (tensile and beam): (a) front view; (b) oblique view

Fig. 5. Specimen geometry: (a) tensile specimens; (b) beams; (c) detail of the existing transverse weld, its removal and the new transverse weld (common for tensile specimens and beams, dimensions in mm)

Fig. 6. Testing set-up for the beams (dimensions in mm)

Fig. 7. Schematic representation of observed failure modes and fracture surface illustration of representative specimens: (a) Failure mode I (tensile specimens); (b) Failure mode I (beams); (c) Failure mode II; (d) Failure mode III

Fig. 8. Experimental data and regression curves.

Fig. 9. General geometry and boundary conditions of FE models (longitudinal section geometry applies to both 2D and 3D models).

Fig. 10. The simplified longitudinal section geometry of the FE parametric models superimposed on the section of specimen T7.

Fig. 11. Discretization of the 3D: (a) global model; sub model at (b) weld toe region T; (c) weld root region R1; (d) weld root region R2

Fig. 12. Exact location of local stress calculation for the application of the CD-PM

Fig. 13: Calculated 5% characteristic fatigue strength for nominal stress range: (a) for the weld toe as a function of $t_b + t_{c2}$; (b) for the weld root as a function of t_{c1}/t_{c1} and t_b

Fig. 14: Recommendations for the geometry of the transverse weld preparation

Table 1. Loading parameters for the tensile specimens.

Specimen	F_{min} [kN]	F_{max} [kN]	$\Delta F/A$ [MPa]	$\Delta\sigma$ [MPa]	f [Hz]
T1	36.4	363.4	145.2	152.3	7
T1**	40.0	400.0	159.9	149.8	6
T2	50.0	500.0	199.8	193.4	5
T3	50.0	500.0	199.8	193.2	5
T4	50.0	500.0	199.8	208.1	5
T5	37.5	375.0	149.9	142.3	7
T6	37.5	375.0	149.9	149.8	7
T6**	50.0	500.0	199.8	196.8	5
T7	40.0	400.0	159.9	167.1	6
T8	40.0	400.0	159.9	178.6	6
T9	50.0	500.0	199.8	199.8*	5
T10	40.0	400.0	159.9	159.9*	6

* It has not been possible to obtain reliable strain measurements for these specimens.
** Indicates run-out specimen retested at a higher stress range

Table 2. Loading parameters for the beam specimens.

Specimen	M_{min} [kNm]	M_{max} [kNm]	$\Delta M/W_{add}$ [MPa]	$\Delta\sigma$ [MPa]	f [Hz]

B1	10.375	103.75	152.0	151.4	6
B2	8.399	83.99	123.3	123.3*	7

*It has not been possible to obtain reliable strain measurements for this specimen.

Table 3. Experimental $\Delta\sigma - N$ results (for failure modes explanation, see Fig. 7).

Specimen	Welding position	$\Delta\sigma$ [MPa]	N	Failure mode
T1	Flat	152.3	7'217'445	Run-out
T6	Flat	149.8	7'217'384	Run-out
T1'	Flat	149.8	397'948	Ia
T6'	Flat	196.8	634'535	II
T5	Flat	142.3	1'739'580	Ia
T7	Flat	167.1	634'535	Ia
T8	Flat	178.6	573'339	Ia
T10	Flat	159.9	3'112'543	III
T2	Flat	193.4	454'857	Ia
T3	Flat	193.2	386'612	Ia
T9	Flat	199.8	292'421	III**
T4	Flat	208.1	285'897	II
B2	Overhead	123.3	1'492'995	Ib*
B1	Overhead	151.4	919'799	Ib*

*On the tension flange.
**Some of the cracks initiated from air inclusions at the root of the weld

Table 4. Statistical analysis results.

set	**analysis**	***n***	***m***	***C***	***s***	$\Delta\sigma_C$ [MPa]	$\Delta\sigma_{C,0.05}$ [MPa]
1	*m* unknown	5	4.51	15.90	0.06	135.2	120.8
	m fixed	5	**3.00**	12.53	0.10	119.2	101.2
2	*m* unknown	7	3.25	13.05	0.09	120.7	101.5
	m fixed	7	**3.00**	12.51	0.09	117.8	103.4
3	*m* unknown	7	5.93	19.18	0.21	147.6	120.8
	m fixed	7	**3.00**	12.59	0.25	124.7	86.0
4	*m* unknown	9	3.73	14.19	0.23	129.9	94.4
	m fixed	9	**3.00**	12.56	0.22	122.3	89.1
5	*m* unknown	12	3.60	13.88	0.22	127.2	94.1
	m fixed	12	**3.00**	12.54	0.21	119.8	88.8

Bold indicates, if any, the fixed parameter in statistical analysis

Table 5. Parametric analysis results from 3D FE models.

case	t_{c1}/t_b	t_{c2}/t_{c1}	t_b [mm]	t_{c1} [mm]	t_{c2} [mm]	e [mm]	D [mm]	L [mm]	d [mm]	3D T $\sigma_{11,PM}$ [SCF]	3D T $\Delta\sigma_{C,0.05}$ [MPa]	3D R1 $\sigma_{11,PM}$ [SCF]	3D R1 $\Delta\sigma_{C,0.05}$ [MPa]	3D R2 $\sigma_{11,PM}$ [SCF]	3D R2 $\Delta\sigma_{C,0.05}$ [MPa]
1		1/2	10	12	6	11	1.0	4		**1.405**	**96**	1.312	103	1.217	111
2			25	30	15	20	1.5	6		1.582	85	**1.640**	**82**	1.643	82
3			42	50	25	30	2.5	10		1.699	79	**1.904**	**71**	1.938	70
4		2/3	10	12	8	13	1.0	4		**1.430**	**94**	1.243	109	1.073	126
5	1.20		25	30	20	25	1.5	6		**1.610**	**84**	1.484	91	1.309	103
6			42	50	33	38	2.5	10		**1.721**	**78**	1.691	80	1.486	91
7		3/4	10	12	9	14	1.0	4		**1.449**	**93**	1.226	110	0.877	154
8			25	30	22	27	1.5	6		**1.615**	**84**	1.422	95	1.245	108
9			42	50	37	42	2.5	10		**1.723**	**78**	1.571	86	1.341	101
10		1/2	16	12	6	11	1.0	4	0.05	1.369	99	**1.460**	**92**	1.365	99
11			40	30	15	20	1.5	6		1.643	82	**1.892**	**71**	1.855	73
12			67	50	25	30	2.5	10		1.765	76	**2.229**	**61**	2.197	61
13		2/3	16	12	8	13	1.0	4		**1.464**	**92**	1.338	101	1.164	116
14	0.75		40	30	20	25	1.5	6		**1.651**	**82**	1.639	82	1.433	94
15			67	50	33	38	2.5	10		1.764	77	**1.889**	**71**	1.634	83
16		3/4	16	12	9	14	1.0	4		**1.476**	**91**	1.298	104	0.935	144
17			40	30	22	27	1.5	6		**1.646**	**82**	1.531	88	1.321	102
18			67	50	37	42	2.5	10		**1.758**	**77**	1.728	78	1.466	92

Bold emphasizes for each case the critical site (i.e. with highest SCF, thus lowest charact. nominal fatigue strength)

Table 6. Parametric analysis results from 2D FE models.

case	t_{c1}/t_b	t_{c2}/t_{c1}	t_b [mm]	t_{c1} [mm]	t_{c2} [mm]	e [mm]	D [mm]	L [mm]	d [mm]	2D merged T $\sigma_{11,PM}$ [SCF]	2D merged T $\Delta\sigma_{C,0.05}$ [MPa]	2D coupled T $\sigma_{11,PM}$ [SCF]	2D coupled T $\Delta\sigma_{C,0.05}$ [MPa]	2D coupled R1 $\sigma_{11,PM}$ [SCF]	2D coupled R1 $\Delta\sigma_{C,0.05}$ [MPa]	2D coupled R2 $\sigma_{11,PM}$ [SCF]	2D coupled R2 $\Delta\sigma_{C,0.05}$ [MPa]	2D contact R1 $\sigma_{11,PM}$ [SCF]	2D contact R1 $\Delta\sigma_{C,0.05}$ [MPa]	2D contact R2 $\sigma_{11,PM}$ [SCF]	2D contact R2 $\Delta\sigma_{C,0.05}$ [MPa]
1	1.20		10	12	6	11				1.424	95	1.458	93	1.167	116	1.219	111	1.354	100	1.320	102
11	0.75	1/2	40	30	15	20				1.663	81	1.808	75	1.714	79	1.987	68	2.144	63	2.298	59
12	0.75		67	50	25	30	1.0	4	0.05	1.782	76	1.962	69	2.035	66	2.421	56	2.614	52	2.857	47
4	1.20		16	12	8	13				1.452	93	1.463	92	1.110	122	1.059	127	1.323	102	1.214	111
14	0.75	2/3	40	30	20	25				1.680	80	1.736	78	1.434	94	1.462	92	1.822	74	1.717	79
15	0.75		67	50	33	38				1.800	75	1.881	72	1.638	82	1.705	79	2.162	62	2.057	66

Table 7. Recommended detail categories for the investigated range of thicknesses.

$t_b + t_{c2} \leq 70$ mm & $w_{c2} \leq 15t_{c2}$	$1 \geq \frac{t_{c2}}{t_{c1}} \geq \frac{3}{4}$	$\frac{3}{4} > \frac{t_{c2}}{t_{c1}} \geq \frac{2}{3}$	$\frac{2}{3} > \frac{t_{c2}}{t_{c1}} \geq \frac{1}{2}$
$t_b \leq 20$	FAT 80 (D)	FAT 80 (D)	FAT 80 (D)*
$20 < t_b \leq 30$	FAT 80 (D)	FAT 80 (D)	FAT 71 (D)*
$30 < t_b \leq 50$	FAT 80 (D)	FAT 71 (D)*	FAT 63 (E)*
$50 < t_b \leq 70$	FAT 71 (D)*	FAT 63 (E)*	FAT 56 (E)*

If $t_b + t_{c2} > 70$ mm, then the fatigue strength of the classes **without** an asterisk should be downgraded by one FAT category.
If $w_{c2} > 15t_{c2}$, then the fatigue strength of the classes **with** an asterisk should be downgraded by one FAT category; w_{c2} is the width of the cover plate extension.
Note that the above modifications do not necessarily result in a lower AASHTO category.

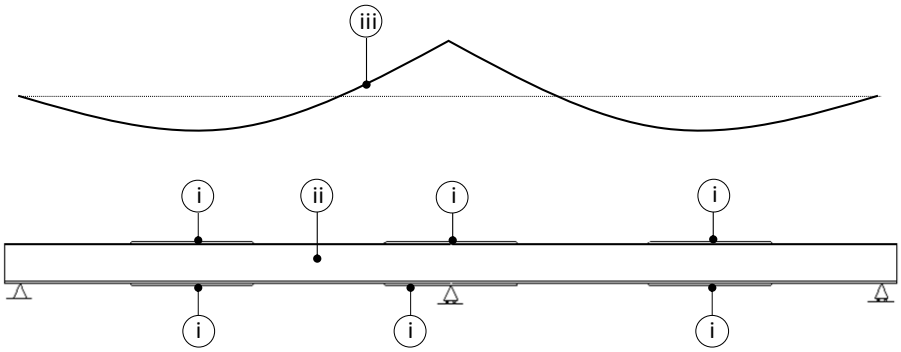

i. Cover plate; ii. Steel girder; iii. Qualitative moment diagram for uniform load

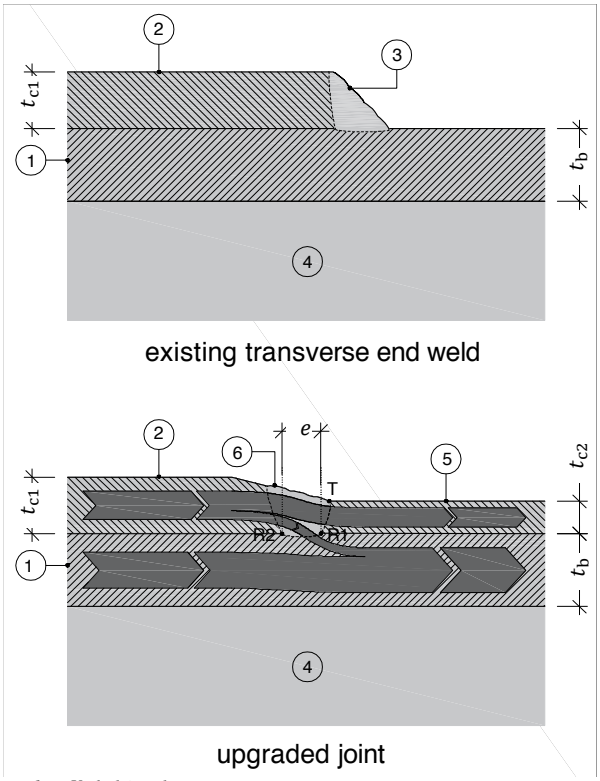

1. *Underlying plate*
2. *Existing cover plate*
3. *Existing transverse end weld*
4. *Web*
5. *Extension cover plate*
6. *New transverse weld*

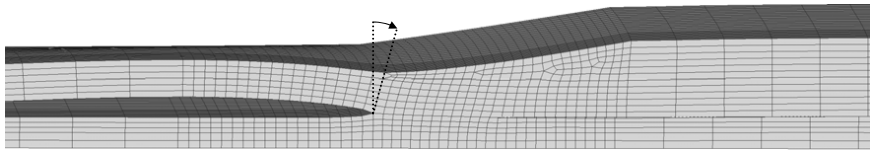

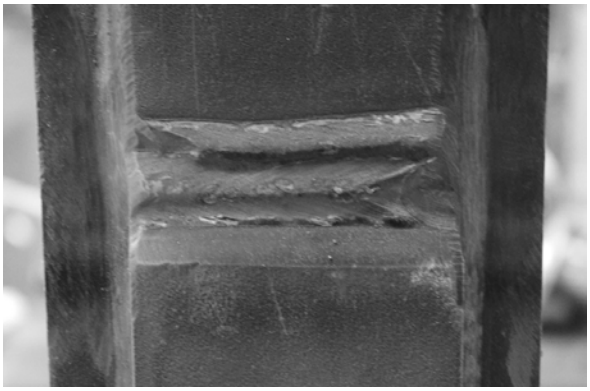

(a)

(b)

(a)

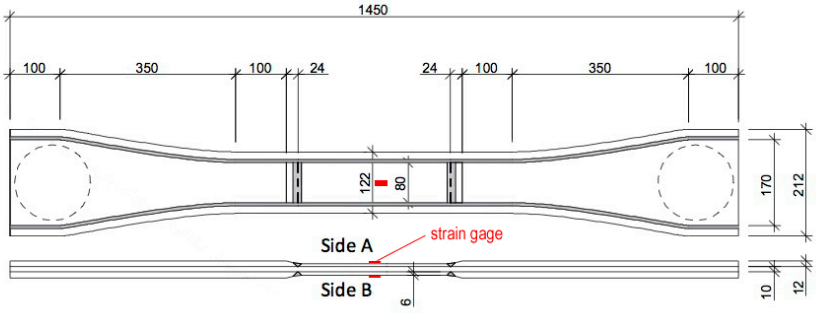
1450
100
350
100
24
24
100
350
100
122
80
170
212
Side A
strain gage
Side B
6
10
12

(b)

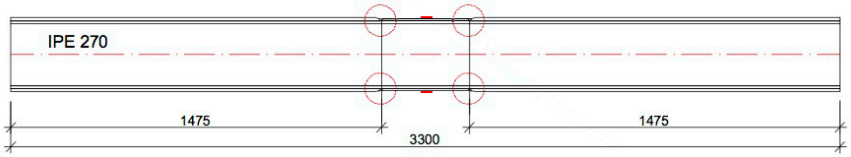
IPE 270
1475
1475
3300

(c)

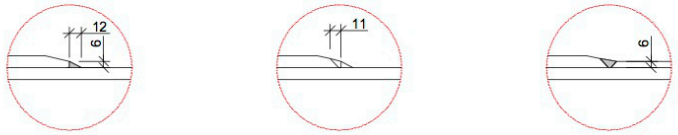
12
6
11
6

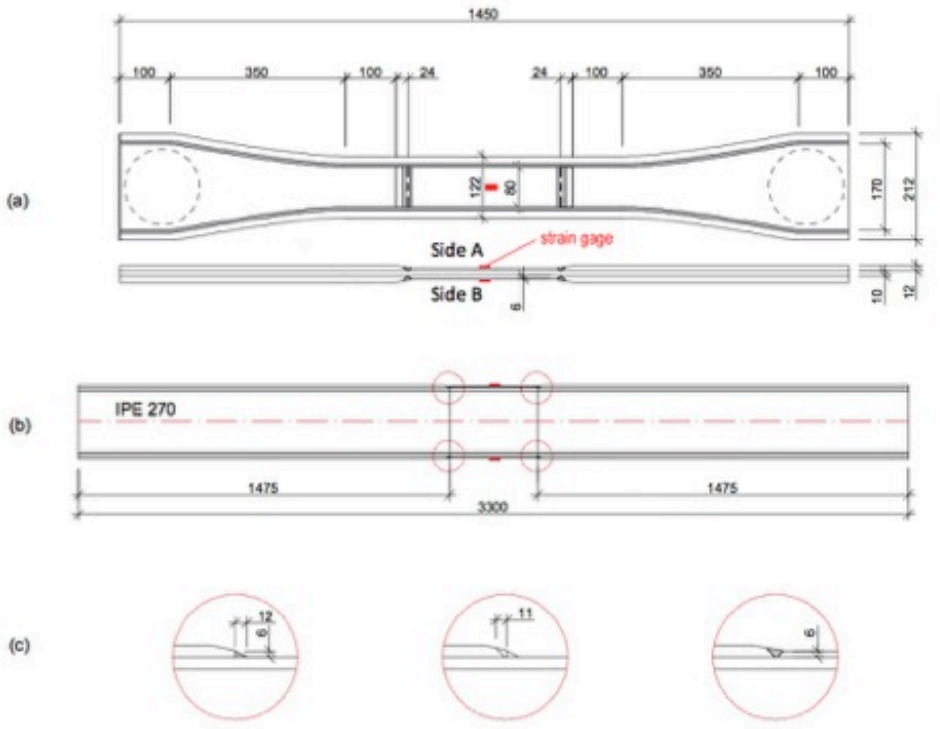
(a)
1450
100
350
100
24
24
100
350
100
122
80
170
212
Side A
strain gage
Side B
6
10
12
(b)
IPE 270
1475
1475
3300
(c)
12
6
11
6

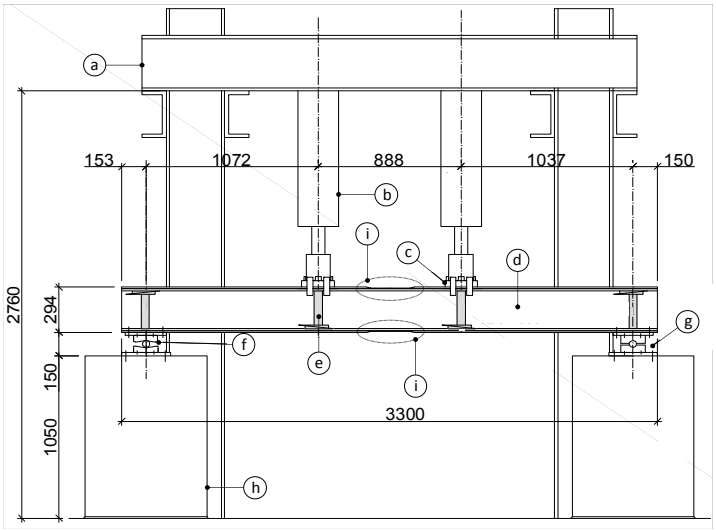

a. Reaction frame

b. Actuator

c. Guiding steel plates (attached to the flange by lindapters)

d. Beam specimen

e. Wooden inserts for web stability

f. Mobile support (bolted on concrete block and beam)

g. Mobile support (bolted on concrete block and beam)

h. Concrete block on mortar layer

i. Location of the joint detail

(a) Failure mode I (tensile specimens)

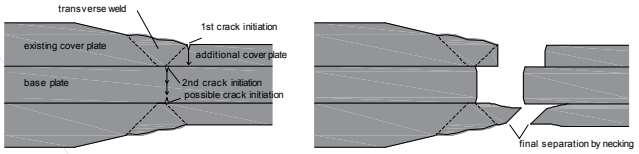

crack initiation and propagation — complete fracture

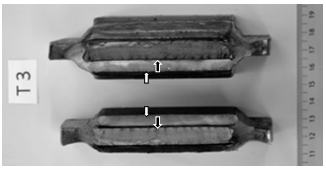

(b) Failure mode I (beams)

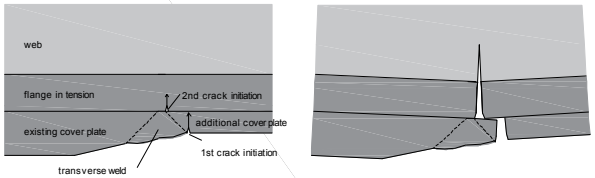

crack initiation and propagation — complete fracture of the flange

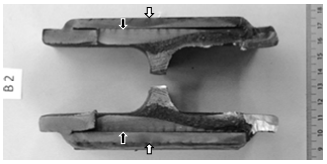

(c) Failure mode II

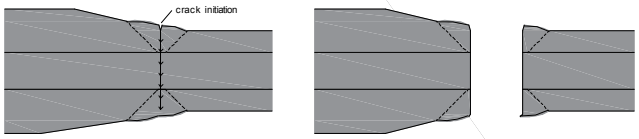

crack initiation and propagation — complete fracture

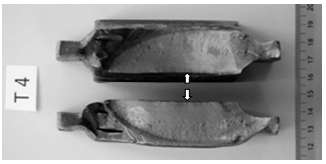

(d) Failure mode III

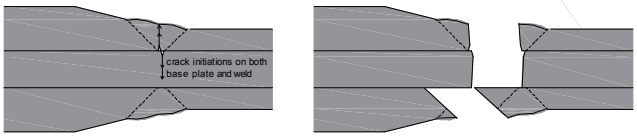

crack initiation and propagation — complete fracture

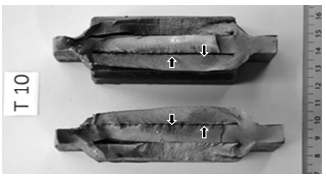

⇩ Root initiation
⇩ Toe or interpass initiation

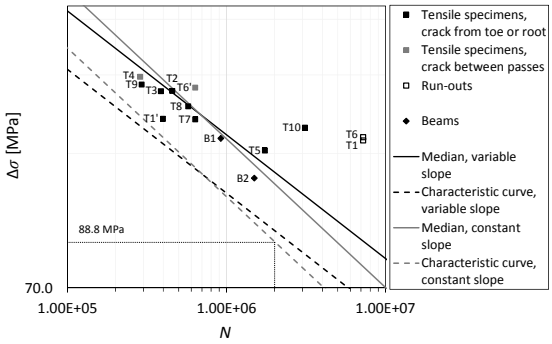
Δσ [MPa]
70.0
1.00E+05
1.00E+06
1.00E+07
N
88.8 MPa
T4
T9
T3
T2
T6'
T8
T7
T1'
B1
T10
T6
T1
T5
B2
Tensile specimens, crack from toe or root
Tensile specimens, crack between passes
Run-outs
Beams
Median, variable slope
Characteristic curve, variable slope
Median, constant slope
Characteristic curve, constant slope

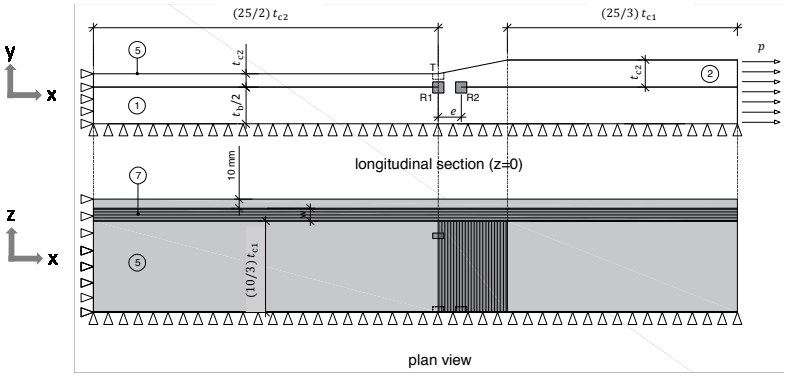

1. *Underlying plate*
2. *Existing cover plate*
5. *Extension cover plate*
1. *Longitudinal weld*

2D: $$p = \frac{2t_{c2} + t_b}{2t_{c1} + t_b} 100\ MPa$$

3D: $$p = \frac{2t_{c2}d + t_b(d + w + 10\ \text{mm}) + 2w^2}{2t_{c1}d + t_b(d + w + 10\ \text{mm}) + 2w^2} 100\ MPa$$

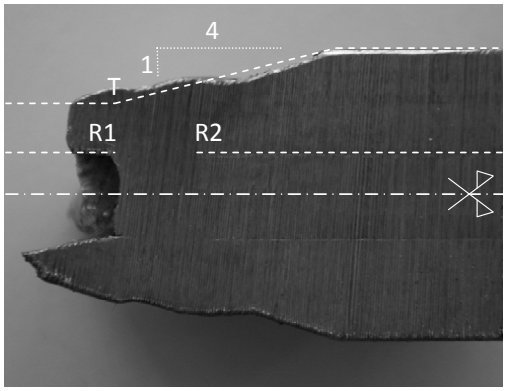
4
1
T
R1
R2

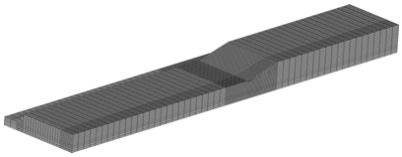

(a)

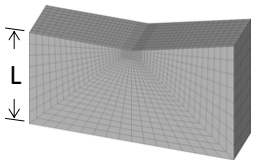

(b)

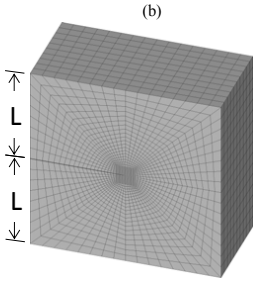

(c)

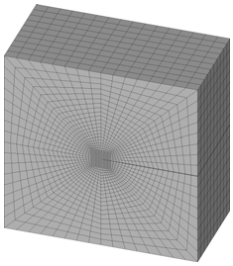

(d)

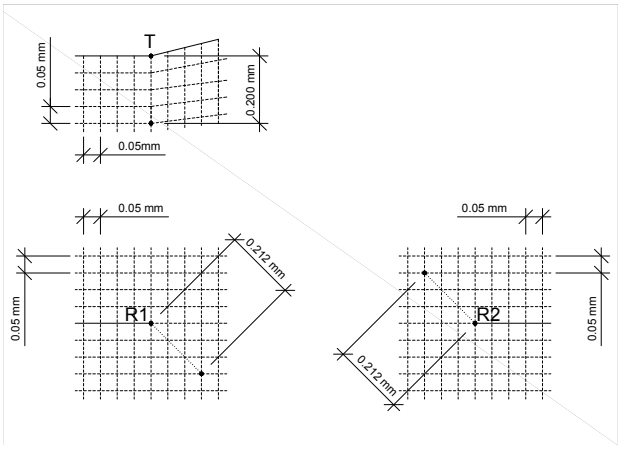
T
0.05 mm
0.200 mm
0.05mm
0.05 mm
0.212 mm
0.05 mm
R1
0.05 mm
R2
0.05 mm
0.212 mm

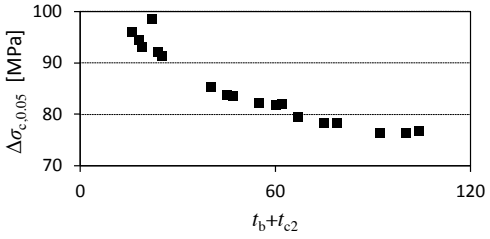
100
90
80
70
$\Delta\sigma_{c,0.05}$ [MPa]
0
60
120
t_b+t_{c2}

(a)

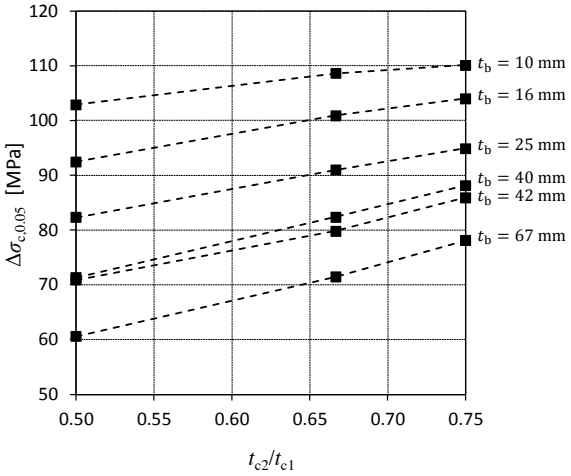
120
110
100
90
80
70
60
50
$\Delta\sigma_{c,0.05}$ [MPa]
0.50
0.55
0.60
0.65
0.70
0.75
t_{c2}/t_{c1}
t_b = 10 mm
t_b = 16 mm
t_b = 25 mm
t_b = 40 mm
t_b = 42 mm
t_b = 67 mm

(b)

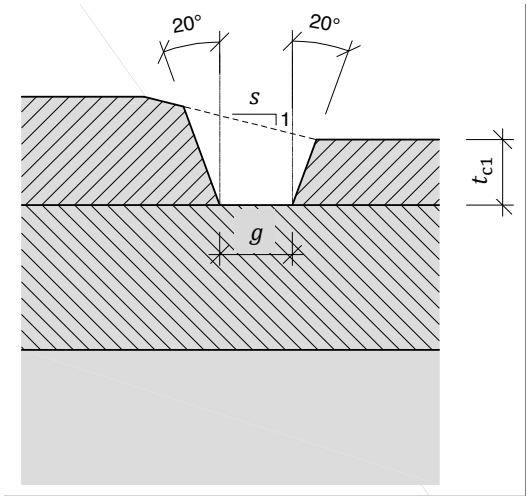

$g \cong t_{c2}, \quad s > 4$